Research Article | Vol. 31, No. 12 / 5 Jun 2023 / Optics Express 19392
Optics EXPRESS

Simple spatially resolved period measurement of chirped pulse compression gratings

FLORIAN BIENERT,* CHRISTOPH RÖCKER, THOMAS GRAF, AND MARWAN ABDOU AHMED

Universität Stuttgart, Institut für Strahlwerkzeuge (IFSW), Pfaffenwaldring 43, 70569 Stuttgart, Germany
florian.bienert@ifsw.uni-stuttgart.de

Abstract: We present an easy-to-implement and low-cost setup for the precise measurement of the period chirp of diffraction gratings offering a resolution of 15 pm and reasonable scan speeds of 2 seconds per measurement point. The principle of the measurement is illustrated on the example of two different pulse compression gratings, one fabricated by laser interference lithography (LIL) and the other by scanning beam interference lithography (SBIL). A period chirp of 0.22 pm/mm^2 at a nominal period of 610 nm was measured for the grating fabricated with LIL, whereas no chirp was observed for the grating fabricated by SBIL, which had a nominal period of 586.2 nm.

1. Introduction

Since its invention in 1985 [1] the technique of chirped pulse amplification (CPA), which was awarded the Nobel prize 2018, is the driver of the scaling of the peak power of ultrafast lasers [2,3]. High-quality diffraction gratings [4] are the key components of the typically used Treacy-compressors [5] driving the technology to unprecedented peak powers. The crucial lithography step in the production of the gratings defines the homogeneity and the quality of their structure. When using optical techniques, lithography is typically based on either laser interference lithography (LIL) [6,7] or scanning beam interference lithography (SBIL) [8,9]. The main difference between the two technologies (and also the reason why SBIL was invented in the first place [10]) is the achievable accuracy of the grating period over a large area. LIL suffers from the period chirp [11,12], which means a spatial inhomogeneity of the grating period i.e. a parabolic increase of the grating period from the center of the substrate to its edge which is accompanied by an inclination of the grating lines [13]. Although the magnitude of the chirp can be reduced by adapting the setup, such adaptions are limited by practical limitations, as they require the operation in vacuum, powerful lasers, and large optics or large distances between the source and the substrate. While the period chirp can largely be avoided with SBIL, the technical implementation is more challenging. Since the interference pattern needs to be scanned precisely over the entire substrate, the machines become significantly more expensive [8]. Depending on the manufacturing technology (LIL or SBIL) and their specific implementations [4,14–18], the change of the period from the substrate's center to the edges can therefore range from fractions of nanometers to a few nanometers. Especially the accurate measurement of small changes in the sub-nm range is a challenging metrological task.

The most commonly used method for measuring the grating period is based on the measurement of the Littrow-angle [19–22]. Thereby the grating is exposed to a laser beam and rotated such that the radiation emitted into the -1st diffraction order (DO) is guided back to the incident beam (Littrow-condition). The accuracy of the measurement strongly depends on the accuracy of the used rotary stage and the involved optical distances (i.e. between the grating and the

#489238 https://doi.org/10.1364/OE.489238
Journal © 2023 Received 6 Mar 2023; revised 10 May 2023; accepted 15 May 2023; published 25 May 2023

Optics EXPRESS

sensor). By employing additional improvements and by using multiple diffraction orders from possibly multiple lasers, the most precise measurements can be achieved with this technique, reporting uncertainties of only 7 pm [23]. The Littrow-approach is therefore used by many national metrology facilities e.g. in Germany, Canada, Switzerland, and Taiwan [24]. A major drawback of this technique is however the extremely long measurement time and the high costs of the setup, especially for the rotary stage. Furthermore, the eccentricity effect [25], meaning that the grating surface is not perfectly located on the axis of rotation, is a persistent problem. This issue was solved by implementing an additional retro-reflector for the rotation [25–28]. Relative measurement errors of $\Delta N/N$ of 3.8×10^{-5} (meaning $\Delta N = 58$ pm for $N = 1536$ nm) [27] and $\Delta N/N$ of 4.99×10^{-5} (meaning $\Delta N = 42$ pm for $N = 833$ nm) [26] were reported using this adaption. While the eccentricity effect could be eliminated, the limitation by the trade-off between the accuracy and the costs of the rotary stage remains present. Another common technique is the so-called "Long Trace profiler" (LTP) which is based on the pencil-beam interferometer of Von Bieren [29]. LTPs rely on the scanning of the grating surface and the sensitive detection of angular changes of one or more DOs [30–33]. For this technique, the planarity of the gratings and the tilt-free movement of the linear stages are of high importance. Both an eventual curvature of the grating and tilting of the linear stages will otherwise influence the angle of incidence of the beam on the grating. This in turn affects the angle of diffraction which leads to possibly large errors in the determination of the grating period. To exclude measurement errors from these sources, the scanning optics should be precisely monitored [33]. With this approach measurement accuracies in the order of 0.3 nm were reported [30].

For the measurement of the grating period also exotic techniques such as e.g. using a mode-locked femtosecond laser [34] or a Talbot interferometer [35] were proposed. Besides these passive approaches where the grating period is determined from the angles of diffraction, direct measurements of the period are used as well. Atomic force microscopes (AFMs), scanning probe microscopes (SPMs), or electron microscopes enable the determination of the grating period without averaging over thousands to millions of grating lines (depending on the beam diameter on the grating) and additionally allow for the determination of the grating depth and shape [23,36,37]. While these techniques provide detailed information on the microscopic properties of the grating, they are in general not suited to measure macroscopic objects on the order of centimeters within a reasonable amount of time [38]. A good overview of some of these methods as well as some other approaches can be found in the publication of Shimizu [39].

The comparison of the different setups shows that the resolution scales with the effort and costs. When employing the widely-used period measurement based on the determination of the Littrow angle, for example, the resolution scales with the accuracy of the rotation stage, and thus the costs. Meanwhile, the speed of the measurement is inversely proportional to the resolution. In this contribution, we present a simple, low-cost, and robust measurement technique that is especially suited to accurately measure the period chirp of pulse compression gratings while only using a few standard off-the-shelf components. It combines the best aspects of several other setups to make it simple, fast (~2 s per measured point), and precise (5 to 15 pm accuracy). The underlying concept is an adaption of an LTP, since this technique generally allows for the fastest measurements and is especially suited to measure relative changes in the period rather than absolute values. Furthermore, it allows for the implementation of large samples while the requirements on the mechanical implementation are comparatively low. As discussed in more detail below, the high precision is obtained by exploiting the sensitivity of the angle of diffraction on the grating period, while the high robustness is achieved by monitoring the 0^{th} DO to eliminate the influences of various errors. The setup, the data processing, and the accuracy are presented and discussed on the example of two exemplary analyzed pulse compression gratings for the NIR spectral range (1030 nm) whereby one grating was fabricated by means of LIL and the other grating by SBIL. Originating from two different manufacturers, the first had a grating period

Optics EXPRESS

of 610 nm and a size of 75 mm × 50 mm (width × height) while the latter grating had a grating period of 586.2 nm and a size of 80 mm × 40 mm (width × height).

2. Measurement setup and methodology

The measurement is performed in two steps. The first measurement serves to determine the absolute grating period at the center of the grating. The second measurement, which constitutes the main part of the present publication, is a spatially-resolved measurement of the period's deviation from the value measured at the center of the grating in the first step. This deviation of the period as a function of space directly translates to the period chirp.

The first measurement can be carried out with any of the established techniques described above. For the measurements presented in this paper, we used the determination of the Littrow angle [20] due to its simple implementation. The main measurement, executed in the second step, was based on an LTP and is schematically shown in Fig. 1(a). The beam of a narrow-banded fundamental-mode continuous-wave (cw) NIR laser illuminates the grating at a defined angle of incidence (AOI) θ_{inc}. The beam of the -1st DO (shown in red) emerges under an angle θ_{-1} and is propagated through a beam splitter and a lens onto a CCD-chip, cf. Figure 1(a). Additionally, the beam of the 0th DO (shown in purple) is also guided to the beam splitter and fed through the lens onto the CCD-chip but with a slight displacement with respect to the beam from the -1st DO. This is shown by the two beam spots depicted in the small insert in the top left corner of the figure. The elongation of the spot of the -1st DO in the direction of diffraction is attributed to the beam's spectral bandwidth.

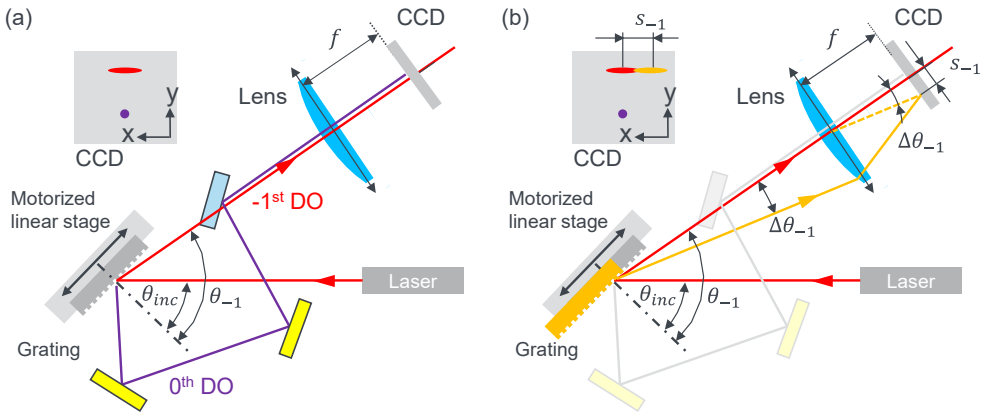

Fig. 1. LTP-based setup used for the determination of the spatial variation of the grating period across the surface of the substrate. Linear stages are used to move the grating parallel to its surface effectively scanning the beam over its surface. The beams of the 0th and the -1st DO are focused on a CCD-chip by means of a lens. (a): In the first step the absolute period of the grating is measured at a fixed position without moving the grating. The square inserted in the top left corner represents the CCD-chip with the two spots originating from the beams in the 0th and the -1st DO. (b): A movement of the period-chirped grating leads to a change in the angle of the -1st DO (orange) with respect to the one measured in the first step (red). The beam path of the 0th DO is greyed out as it is not directly needed for this second measurement step. It is however used to detect potential tilting of the grating's surface and therewith increase the precision of the measurement.

To measure the period chirp, the grating is moved parallel to its surface with two motorized linear stages for horizontal and vertical displacement. In the presence of a chirped period, a change in the position on the grating leads to a change in the period affecting the laser beam. This in turn leads to a change in the diffraction angle, as depicted by the orange beam in Fig. 1(b).

Optics EXPRESS

Since the CCD-chip is located at a distance of the focal length f from the lens, the change in the diffraction angle $\Delta\theta_{-1}$ can be calculated from the shift s_{-1} of the beam on the CCD-chip. For a precise determination of the local deviation of the grating period one however needs to take into consideration the error that would be caused by any existing curvature of the grating's surface or possible angular errors introduced by the linear stage. To correct these errors, the 0^{th} DO is tracked to detect any changes in the AOI by measuring the shift s_0 of the spot of the 0^{th} DO on the CCD-chip. With a fixed incident laser beam, a change of the AOI by $\Delta\theta_{inc}$ results in a tilt of $2\Delta\theta_{inc}$ of the beam reaching the lens and hence

$$\Delta\theta_{inc} = \frac{1}{2}\arctan\left(\frac{s_0}{f}\right). \tag{1}$$

Taking this possible change of the AOI into account, the change of the angle of diffraction $\Delta\theta_{-1}$ is given by

$$\Delta\theta_{-1} = \Delta\theta_{inc} - \arctan\left(\frac{s_{-1}}{f}\right). \tag{2}$$

Adding this information to the generally known grating equation (for reflection)

$$\sin(\theta_m) = \sin(\theta_{inc}) + m \cdot \frac{\lambda}{\Lambda}, \tag{3}$$

with θ_m being the diffraction angle of the m^{th} diffraction order, the period of the grating is found to be

$$\Lambda = \frac{\lambda}{\sin(\theta^*_{inc}+\Delta\theta_{inc}) - \sin(\theta^*_{-1}+\Delta\theta_{-1})}, \tag{4}$$

where θ^*_{inc} is the nominal angle of incidence as set and θ^*_{-1} the resulting diffraction angle determined in the first reference measurement. By expressing θ^*_{-1} with the period Λ^* determined in the first reference measurement, Eq. (5) is transformed to

$$\Lambda = \frac{\lambda}{\sin(\theta^*_{inc}+\Delta\theta_{inc}) - \sin\left(\sin^{-1}\left(\sin(\theta^*_{inc}) - \frac{\lambda}{\Lambda^*}\right) + \Delta\theta_{-1}\right)}. \tag{5}$$

In order to detect the smallest possible changes in the grating period, the measurements need to be carried out for an AOI at which the diffraction angle depends very sensitively on the period. In mathematical terms, this means that $d\theta_{-1}/d\Lambda^*$ should adopt a large value. This can be achieved by suitably choosing either the wavelength or the AOI of the probe beam. To find a suitable AOI, the grating equation (Eqn. (3)) may be solved for θ_{-1} and its derivative

$$\frac{\mathrm{d}\theta_{-1}}{\mathrm{d}\Lambda^*} = \frac{\lambda}{(\Lambda^*)^2 \cdot \sqrt{1 - \left(\sin(\theta^*_{inc}) - \frac{\lambda}{\Lambda^*}\right)^2}} \tag{6}$$

is calculated with respect to the nominal period Λ^* measured in the reference measurement at the center of the grating. Figure 2 shows the angle of diffraction θ_{-1} of the -1^{st} DO and its sensitivity $\mathrm{d}\theta_{-1}/\mathrm{d}\Lambda^*$ as a function of the angle of incidence θ^*_{inc} for a nominal period of $\Lambda^* = 610$ nm (corresponding to the LIL-based grating) and a probing wavelength of $\lambda = 1030$ nm. Although other wavelengths would also have been suitable for the measurement this wavelength was chosen because such a laser was available. The two curves in Fig. 2 show that the operation of the grating close to the cut-off angle of the -1^{st} DO ($|\theta_{-1}| > 90°$) significantly increases the sensitivity. For the experimental characterization of the chirped LIL grating an AOI of $\theta^*_{inc} = 44°$ ($\theta_{-1} = -83.65°$) was therefore chosen (see orange dash-dotted line) yielding a sensitivity of $\mathrm{d}\theta_{-1}/\mathrm{d}\Lambda^* = 1.43$ °/nm. This approach led to an increase of the sensitivity and thus of the accuracy by a factor of approximately 5 compared to setups that operate under the Littrow-condition (see the black dashed line, $\mathrm{d}\theta_{-1}/\mathrm{d}\Lambda^* = 0.3$ °/nm).

Optics EXPRESS

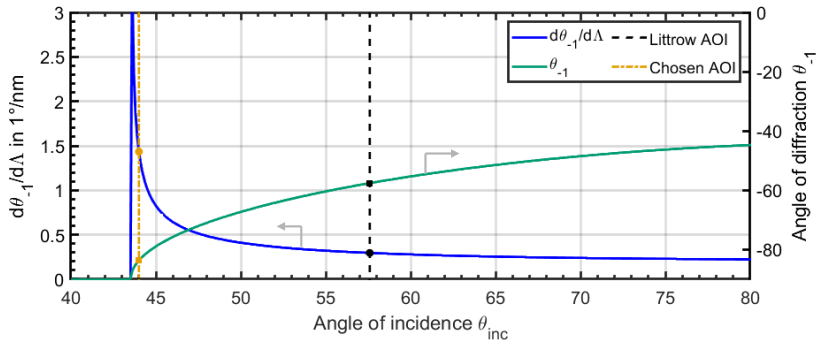

Fig. 2. Dependence of the sensitivity $d\theta_{-1}/d\Lambda^*$ on the AOI for the LIL grating with a nominal period of $\Lambda^* = 610$ nm. The configuration depicted by the yellow dash-dotted line was chosen.

3. Data processing and results

Figure 3 shows the grayscale image recorded by the CCD-chip during the reference measurement at the center ($x = y = 0$) of the LIL grating. The upper and lower white spots correspond to the beams of the -1st DO and 0th DO, respectively. The horizontal elongation of the -1st DO is attributed to the spectral bandwidth of the laser beam which was measured to be $\Delta\lambda = 166$ pm (FWHM).

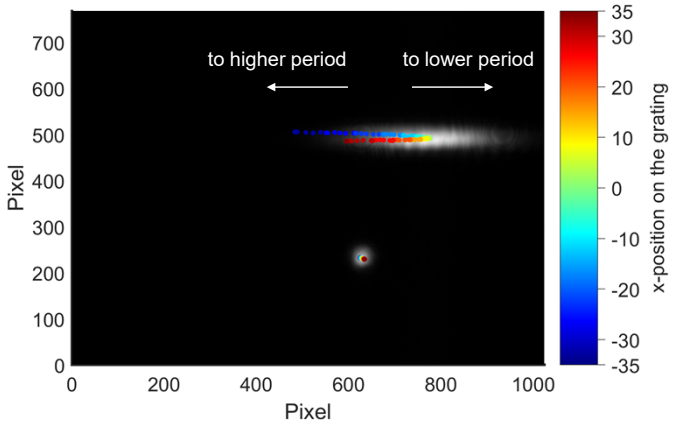

Fig. 3. Picture obtained on the CCD-chip (grayscale) with the spot of the 0th DO (bottom) and the one of the -1st DO (top) overlayed by the measured centers of gravity of these spots (in color) obtained when scanning the grating as depicted in Fig. 1.

When the chirped grating is moved perpendicular to the grating lines as depicted in Fig. 1, the spot of the -1st DO moves on the CCD-chip due to the spatially varying grating period. This is shown by the colored dots, which represent the centers of gravity (COG) of the spots on the chip for different measurement points during the scan along the grating's surface. The color scale indicates their positions (x = 0 at the center corresponding to green color). The movement of the COG to the left indicates that the period increases with increasing distance from the reference point at the center of the grating. Both spots are also shown in Fig. 4 but with higher resolution. The vertical displacement of the COGs of the -1st DO (cf. white arrow in Fig. 4(a)) is attributed to a slight local change in the orientation of the grating lines (as e.g. illustrated by Fig. 9 in Ref. [13]). The smaller displacement of the COGs of the 0th DO (cf. Figure 4(b)) is attributed

Optics EXPRESS

to the (unwanted) mechanical tilting of the stage upon movement and an eventual waviness of the grating's surface. For the measurement, the beam was collimated with a diameter of 2 mm. Since the position of the beam is obtained by the COG via the momentum method the divergence and beam diameter are of low importance.

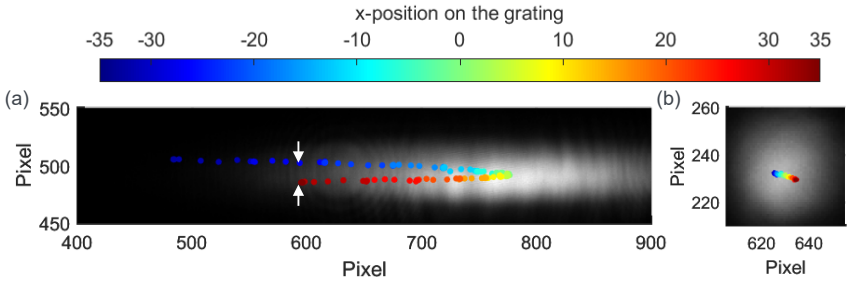

Fig. 4. (a): Enlarged excerpt of the spot of the -1st DO from Fig. 3. (b): Enlarged excerpt of the spot of the 0th DO from Fig. 3.

Figure 5(a) shows the spatially resolved period of the two different (LIL and SBIL) pulse compression gratings along two different lines through their center, i.e. once along a direction perpendicular (⊥) and once parallel (||) to the grating lines. The measurements were obtained

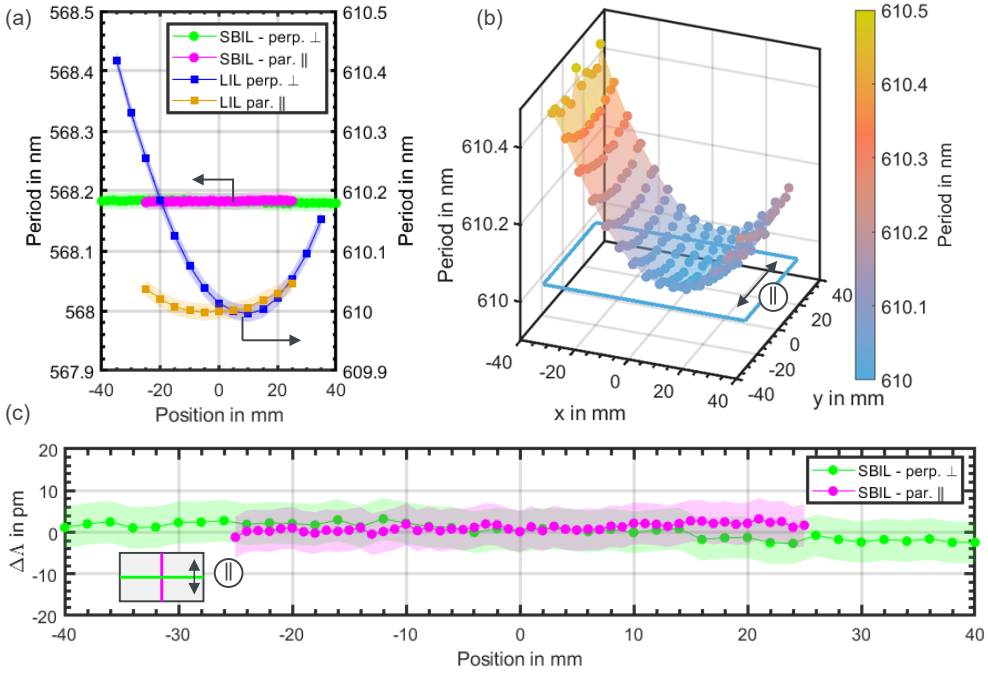

Fig. 5. (a): Measured period of the two gratings along the direction perpendicular (⊥) and parallel (||) to the grating lines through the center. (b): Measured period of the LIL grating across the whole surface. The black arrow indicates the orientation perpendicular to the grating lines. (c): Magnified presentation of the measured period of the SBIL grating. The black arrow in the insert in the bottom left corner shows the orientation perpendicular to the grating lines with respect to the lines along which the measurements were carried out on the grating surface.

Optics EXPRESS

using equations Eqn. (1), (2), and (5) and inserting the values s_{-1} and s_0 corresponding to the displacements of the COG of the spots recorded on the CCD chip.

The grating fabricated by LIL shows the typical parabolic spatial dependence [13] of the period. The asymmetry of the spatial period variation furthermore indicates that the interference pattern used to fabricate the grating, cf., Refs. [13,40], was not perfectly centered on the sample. This can be seen in more detail in Fig. 3(b) where a full scan of the sample is shown. To quantify the observed chirp, we consider the quadratic period chirp as defined by the second derivatives $\chi_\perp = d^2\Lambda/dx^2$ for the perpendicular direction ($\perp$) and $\chi_\parallel = d^2\Lambda/dy^2$ for the parallel direction ($\parallel$). This definition is advantageous since the distribution of the grating's period typically follows a parabolic spatial dependence [13,40]. By applying quadratic fits and extracting the quadratic terms, period chirps of $\chi_\perp$ =0.22 pm/mm^2 and $\chi_\parallel$ =0.077 pm/mm^2 were determined for the respective directions. As shown in Fig. 5(a) and with a larger magnification in Fig. 5(c) no apparent spatial variation of the period is observable for the grating fabricated with SBIL. The shaded areas shown both in Fig. 5(a) and Fig. 5(c) represent the calculated accuracy of the measurement as discussed in the following section.

4. Measurement accuracy

The measurement accuracy of our setup is discussed exemplary for the case of the grating that was fabricated by LIL. The measurement of the spatial dependence of the grating's period in the direction perpendicular to the grating lines through the center of the sample (depicted in blue in Fig. 5(a)) is considered for the following analysis. This analysis is performed on this measurement since it exhibits the largest change of the period and since its raw data was already shown in Fig. 3 and Fig. 4. In order to determine the uncertainty of our measurement, we first analyze the uncertainty of the determination of the angles $\alpha_0 = 2\Delta\theta_{inc} = \arctan(s_0/f)$ and $\alpha_{-1} = \arctan(s_{-1}/f)$, cf equation Eqn. (1) and (2). To calculate the error propagation, we consider the whole optical setup comprising the grating, the propagation distance l' along the -1st DO to the lens, the lens with the focal length f and the length l from the lens to the CCD chip. Table 1 lists the values of these parameters and their assumed uncertainties used for the error propagation to determine the resulting overall uncertainty of α_0 and α_{-1}. The values of the shifts s_0 and s_{-1} correspond to the maximum values observed on the CCD-chip, as depicted in Fig. 4. The error in the determination of their COG (e.g., due to eventual camera noise) was derived to 0.1 pixel from repeated measurements. However, it was rather conservatively specified to be about half a pixel to also include effects originating from the collimation of the beam, i.e. beam diameter and divergence, as well as the movement of the beam on the lens. The latter creates an astigmatism of the beam and could lead to an error in the determination of the beam's COG. Since this movement is in the range of 1 mm at max, the error is considered to be minor and is included in the specified error of half a pixel. For the lens, the uncertainty in the focal length was accounted to 1 mm. Eventual astigmatism and spherical aberrations of the lens were not measured and are therefore simply included in both the uncertainty of the determination of the beam's COG and the focal length of the lens.

The lower part of Table 1 shows that the calculated relative errors of α_0 and α_{-1} amount to 6% and 0.7%, respectively. The higher (relative) uncertainty for the 0th DO results from the small movement of the spot with respect to the unchanged absolute uncertainty of the half pixel. The calculation of the error propagation for the grating period was then performed in a second step using the uncertainty of α_0 and α_{-1} together with the equations Eqn. (1), (2), and (5). The values and uncertainties of the used parameters are listed in Table 2.

Assuming a perfectly known period resulting from the first reference measurement (Case A) the maximum uncertainty of the determined period (which occurs when the diffracted beam experiences its maximum shift on the CCD-chip (x = –35 mm, y = 0 mm) was determined to be 15 pm (see lower part of Table 2). Although smaller errors occur for points with lower period

Optics EXPRESS

Table 1. Parameters and their uncertainties (upper part) used to calculate the expected uncertainties of α_0 and α_{-1} (lower part).

Parameter	Symbol	Nominal Value	Uncertainty
Distance lens and grating for 0th DO	l'_0	250 mm	10 mm
Distance lens and grating for -1st DO	l'_{-1}	745 mm	10 mm
Distance lens and CCD-Chip	l	185 mm	1 mm
Focal length	f	185 mm	1 mm
Shift of the beam on the CCD-Chip for 0th DO	s_o	15·4.65 µm	0.5·4.65 µm
Shift of the beam on the CCD-Chip for -1st DO	s_{-1}	300·4.65 µm	0.5·4.65 µm
Results			
Angular change of the 0th DO	α_0	0.38 mrad	23 µrad = 6%
Angular change of the -1st DO	α_{-1}	7.5 mrad	53 µrad = 0.7%

Table 2. Parameters and their uncertainties (upper part) used to calculate the expected uncertainties of the period Λ and the chirp $\chi_\perp$ (lower part). Three different uncertainties of the reference period Λ^* are considered, described by the cases A, B and C

Parameters	Symbol	Nominal Value	Uncertainty
Wavelength		1030 mm	0.1 nm
Nominal angle of incidence	θ^*_{inc}	44°	$12° \cdot 10^{-3}$
Angular change of the 0th DO	α_0	0.38 mrad	23 µrad = 6%
Angular change of the -1st DO	α_{-1}	7.5 mrad	53 µrad = 0.7%
Nominal period (Case A - Ideal)	Λ^*_A	610 nm	0 pm
Nominal period (Case B - PTB [23])	Λ^*_B	610 nm	10 pm
Nominal period (Case C - Our setup)	Λ^*_C	610 nm	100 pm
Results			
Period at max point (Case A - Ideal)	Λ_A	610.41 nm	15 pm
Period at max point (Case B - PTB [23])	Λ_B	610.41 nm	26 pm
Period at max point (Case C - Our setup)	Λ_C	610.41 nm	124 pm
Period Chirp at max point (Case A, B and C)	$\chi_{A,B,C}$	0.22 pm/mm^2	0.015 pm/mm^2

change (closer to the vertex of the parabola) the uncertainty of 15 pm was adopted to all points shown in Fig. 5(a).

Since in practice the period Λ^* determined by the first reference measurement is also uncertain its influence needs to be considered too using Eqn. (5). Essentially, however, this uncertainty of Λ^* merely leads to a shift of the determined parabola while the opening of the parabola (i.e. the quadratic coefficient and thus the chirp χ) is nearly unaffected. The following simulated example shows this in a quantitative matter. It is supposed the substrate has a nominal period of 610.1 nm at the center and a period of 610.4 nm at the edge. This results in an actual period difference of 0.3 nm from the center to the edge. By incorrectly assuming that the nominal period is 610 nm (at the center) and by applying the presented equations Eqn. (1), (2) and (5) the period at the edge would be determined to be 610.294 nm. This means that the change is found to be 0.294 nm instead of the nominal 0.3 nm, creating an error of only 6 pm, while the nominal period was wrongfully determined by 100 pm (610 nm instead of 610.1 nm). This small influence of the nominal period is reflected in the error propagation for the period for cases B and C. For case B it is assumed that the nominal period is determined with an uncertainty of 10 pm, as it could be achieved by the PTB [23]. This uncertainty results in an absolute error of 26 pm for the

Optics EXPRESS

outermost point (x = –35 mm y = 0 mm), which is mainly the sum of the general error of 15 pm with the additional error of 10 pm from the nominal period. For case C it is assumed that the nominal period is determined with an uncertainty of 100 pm, as our Littrow-Setup is specified. The resulting absolute error of 126 pm is again only slightly higher than the sum of the general error of 15 pm with the additional error of 100 pm.

Since the presented method is designed to measure the period chirp, the uncertainties in the determination of the quadratic coefficients $\chi_\perp = d^2\Lambda/dx^2$ and $\chi_\parallel = d^2\Lambda/dy^2$ is of great importance. They can be determined from the influence of the uncertainties of the period measurements of the individual points onto the fit of the parabolas. For all three cases the uncertainty of the chirp $\chi_\perp$ was determined to be 0.015 pm/mm^2, cf. Table 2. This value also includes the positional error of the stage specified by the supplier as <2 µm for the bidirectional repeatability at a single point and by <16 µm/100 mm for the overall positional error. The independence of the uncertainty of the period chirp from the first reference measurement Λ^* can already be concluded from the simulated example described above. The uncertainty of Λ^* mainly results in the shift of the obtained parabolic spatial distribution of the period while it's opening (defined by the quadratic coefficients) is nearly unaffected.

By applying the presented error propagation on the data of the SBIL grating, an uncertainty of 5 pm was determined. This unprecedented small uncertainty is mainly attributed to the small movement of the beams due to the substrate's high planarity and the extremely homogeneous period.

The obtained deviations of the measurements were observed to be on a much smaller scale than the absolute errors. For the 40-times repeated measurement of a single point (without moving the stage) a standard deviation (STD) of 0.4 pm and a peak-to-valley deviation (PV) of 2 pm were determined which indicates the low errors arising from camera noise and from spectral and pointing fluctuations of the laser.

5. Discussion and outlook

The method presented in this paper combines an absolute measurement of the period with the measurement of a relative period change. The accuracy of the measurements, therefore, needs to be discussed in two parts. The absolute accuracy of our measurement is defined by the accuracy of our Littrow-setup and cannot compete with the state-of-the-art period measurements. For the application (i.e. pulse compression) however, the period chirp i.e. the change of the grating period, is much more important. In the proposed approach this quantity is measured with much higher accuracy, as it exploits the high sensitivity of $d\theta_{-1}/d\Lambda^*$ and uses the 0$^{\text{th}}$ DO to correct errors associated with any changes in the AOI.

For the measurement, the beam was collimated with a diameter of 2 mm. As specified in the previous section, the position of the beam is obtained by the COG via the momentum method. Therefore, the beam's divergence and diameter have only minor influence on the determination of the beam's position on the CCD-chip. However, the beam size results in an averaged measurement of the periods of all grating lines that lie within the diameter of the beam on the grating. When a fine spatial resolution should be obtained, smaller beam diameters are required.

Besides the characterization of pulse compression gratings, our setup is also well-suited for the characterization of other grating-based optics such as phase masks used for the inscription of chirped fiber Bragg gratings [41,42]. Also, other objects that are not initially designed for diffraction can be characterized as long as they show certain periodicity [43] and some power contained in a diffraction order when exposed to a laser beam. Thereby the diffraction efficiency of the sample, as well as the absolute intensity of the beam, are only of minor importance since the position of the beam is obtained by the COG. Because the exposure time of the camera can be adapted for every image, respectively position of the grating, even spatial dependencies of the diffraction efficiency can therefore easily be compensated. This also enables a measurement of

Optics EXPRESS

the grating period during the fabrication, i.e. after the lithography/development and before the etching process. Depending on the wavelength used for the measurement, the exposed photoresist grating already allows for the diffraction of a few percent of the incident radiation.

Concerning our existing setup several improvements are planned and will be part of future efforts. Among others, the focus will be on a full automatization and the real-time processing of the obtained data which should additionally increase the measurement speed. Furthermore, the determination of the inclination of the grating lines is pursued, whose effects were already visible in our measurements. Finally, we will investigate the advantages of using a different laser source with a shorter wavelength to excite more DOs. This can increase both accuracy and precision in two ways. First, the choice of the wavelength influences the sensitivity $d\theta_{-1}/d\Lambda$ as shown in Eqn. (6) and can therefore further enhance the signal-to-noise ratio. Second, the measurement of the spots of more DOs on the camera will lead to a further reduction of the uncertainty as reported in Ref. [22].

6. Conclusion

In summary we presented a low-cost, robust, and easy-to-implement metrological setup based on a long trace profiler (LTP) that is especially suited for the precise and fast measurement of the period chirp. The underlying principle, the theory, and the data treatment of the setup were shown on the example of a period-chirped grating fabricated with LIL and an unchirped grating fabricated with SBIL. The operation of the setup at a condition where the angle of diffraction is very sensitive to the grating period and the simultaneous monitoring of the 0^{th} DO to correct for changes in the AOI allowed for a measurement of period changes with high precision. For the grating fabricated with LIL uncertainties of only 15 pm (period change) for a single point and 0.015 pm/mm^2 (with respect to $\chi_\perp$ =0.22 pm/mm^2) for the period chirp were achieved. For the grating fabricated with SBIL, no chirp was observed, and an uncertainty of unprecedented 5 pm (period change) was achieved.

Funding. Horizon 2020 Framework Programme (825246).

Acknowledgements. This project is an initiative of the Photonics Public Private Partnership from the European Union's Horizon 2020 research and innovation programme under grant agreement No 825246.

Disclosures. The authors declare no conflict of interest

Data availability. Data underlying the results presented in this paper are not publicly available at this time but may be obtained from the authors upon reasonable request.

References

1. D. Strickland and G. Mourou, "Compression of amplified chirped optical pulses," Opt. Commun. **55**(6), 447–449 (1985).
2. C. P. J. Barty, "The Nexawatt: A Strategy for Exawatt Peak Power Lasers Based on NIF and NIF-like Beam Lines," J. Phys.: Conf. Ser. **717**, 012086 (2016).
3. C. N. Danson, C. Haefner, and J. Bromage, *et al.*, "Petawatt and exawatt class lasers worldwide," High Power Laser Sci. Eng. **7**, e54 (2019).
4. N. Bonod and J. Neauport, "Diffraction gratings: from principles to applications in high-intensity lasers," Adv. Opt. Photon. **8**(1), 156 (2016).
5. E. B. Treacy, "Optical Pulse Compression With Diffraction Gratings," IEEE J. Quantum Electron. **5**(9), 454–458 (1969).
6. C. Lu and R. H. Lipson, "Interference lithography: A powerful tool for fabricating periodic structures," Laser Photonics Rev. **4**(4), 568–580 (2010).
7. C. J. M. Van Rijn, "Laser interference as a lithographic nanopatterning tool," J. Micro/Nanolith. MEMS MOEMS **5**(1), 011012 (2006).
8. C. G. Chen, P. T. Konkola, R. K. Heilmann, C. Joo, and M. L. Schattenburg, "Nanometer-accurate grating fabrication with scanning beam interference lithography," Nano- Microtechnology Mater. Process. Packag. Syst. **4936**, 126–134 (2002).
9. C. G. Chen and M. L. Schattenburg, "Beam Alignment and Image Metrology for Scanning Beam Interference Lithography – Fabricating Gratings with Nanometer Phase Accuracy," (2003).

Optics EXPRESS

10. C. G. Chen and M. L. Schattenburg, "A brief history of gratings and the making of the MIT Nanoruler," *J. Vac. Sci. Technol.* 1–10 (2004).
11. A. Katzir, A. C. Livanos, J. B. Shellan, and A. Yariv, "Chirped Gratings in Integrated Optics," IEEE J. Quantum Electron. **13**(4), 296–304 (1977).
12. J. Ferrera, "Analysis of distortion in interferometric lithography," J. Vac. Sci. Technol. B **14**(6), 4009–4013 (1996).
13. F. Bienert, T. Graf, and M. Abdou Ahmed, "Comprehensive theoretical analysis of the period chirp in laser interference lithography," Appl. Opt. **61**(9), 2313–2326 (2022).
14. J. Keck, J. B. Oliver, T. J. Kessler, H. Huang, J. Barone, J. Hettrick, A. L. Rigatti, T. Hoover, K. L. Marshall, A. W. Schmid, A. Kozlov, and T. Z. Kosc, "Manufacture and development of multilayer diffraction gratings," Laser-Induced Damage Opt. Mater. 2005 **5991**, 59911G (2005).
15. S. N. Dixit, J. A. Britten, R. A. Hyde, C. R. Hoaglan, M. C. Rushford, L. J. Summers, and J. S. Toeppen, "Fabrication and applications of large- aperture diffractive optics," Lithogr. Micromach. Tech. Opt. Compon. Fabr. **4440**, 101–108 (2001).
16. H. Korre, C. P. Fucetola, J. A. Johnson, and K. K. Berggren, "Development of a simple, compact, low-cost interference lithography system," J. Vac. Sci. Technol., B: Nanotechnol. Microelectron.: Mater., Process., Meas., Phenom. **28**(6), C6Q20–C6Q24 (2010).
17. J. A. Britten, "In situ end-point detection during development of submicrometer grating structures in photoresist," Opt. Eng **34**(2), 474 (1995).
18. M. Li, C. Zhou, C. Wei, W. Jia, Y. Lu, C. Xiang, and X. Xiang, "Image grating metrology using phase-stepping interferometry in scanning beam interference lithography," Hologr. Diffractive Opt. Appl. VII **10022**, 1002212 (2016).
19. D. A. Brasil, J. A. P. Alves, and J. R. Pekelsky, "An imaging grating diffractometer for traceable calibration of grating pitch in the range 20 μm to 350 nm," J. Phys.: Conf. Ser. **648**, 012013 (2015).
20. J. R. Pekelsky, B. J. Eves, P. R. Nistico, and J. E. Decker, "Imaging laser diffractometer for traceable grating pitch calibration," Meas. Sci. Technol. **18**(2), 375–383 (2007).
21. J. E. Decker, B. J. Eves, J. R. Pekelsky, and R. J. Douglas, "Evaluation of uncertainty in grating pitch measurement by optical diffraction using Monte Carlo methods," Meas. Sci. Technol. **22**(2), 027001 (2011).
22. V. Korpelainen, A. Iho, J. Seppä, and A. Lassila, "High accuracy laser diffractometer: Angle-scale traceability by the error separation method with a grating," Meas. Sci. Technol. **20**(8), 084020 (2009).
23. D. A. Chernoff, E. Buhr, D. L. Burkhead, and A. Diener, "Picometer-scale accuracy in pitch metrology by optical diffraction and atomic force microscopy," Metrol. Insp. Process Control Microlithogr. XXII **6922**, 69223J (2008).
24. J. E. Decker, E. Buhr, A. Diener, B. Eves, A. Kueng, F. Meli, J. R. Pekelsky, S.-P. Pan, and B.-C. Yao, "Report on an international comparison of one-dimensional (1D) grating pitch," Metrologia **46**(1A), 04001 (2009).
25. Q. Wang, Z. Liu, H. Chen, Y. Wang, X. Jiang, and S. Fu, "The method for measuring the groove density of variable-line-space gratings with elimination of the eccentricity effect," Rev. Sci. Instrum. **86**(2), 023109 (2015).
26. B. Sheng, G. Chen, Y. Huang, and L. Luo, "Note: Measuring grating periods by diffraction method with a fore-end light path comprising fused fiber couplers and fiber port collimators," Rev. Sci. Instrum. **88**(10), 106102 (2017).
27. B. Sheng, G. Chen, Y. Huang, and L. Luo, "Measurement of grating groove density using multiple diffraction orders and one standard wavelength," Appl. Opt. **57**(10), 2514 (2018).
28. T. H. Yoon, C. Il Eom, M. S. Chung, and H. J. Kong, "Diffractometric methods for absolute measurement of diffraction-grating spacings," Opt. Lett. **24**(2), 107 (1999).
29. K. von Bieren, "Pencil Beam Interferometer For Aspherical Optical Surfaces," Laser Diagnostics **0343**, 101–108 (1982).
30. J. Lim and S. Rah, "Technique for measuring the groove density of a diffraction grating with elimination of the eccentricity effect," Rev. Sci. Instrum. **75**(3), 780–782 (2004).
31. D. Cocco, R. Sergo, G. Sostero, and M. Zangrando, "High-precision measurements of the groove density of diffraction gratings," Soft X-Ray EUV Imaging Syst. **4146**, 143–150 (2000).
32. Z. R. Wu, T. C. Kao, C. W. Kao, P. C. Chang, W. Lin, and Y. J. Hung, "Wafer-scale grating mapping system for rapid pitch and diffraction efficiency measurement," *OECC/PSC 2019 - 24th Optoelectron. Commun. Conf. Conf. Photonics Switch. Comput. 2019* 1, 2019–2021 (2019).
33. J. Song, R. K. Heilmann, A. R. Bruccoleri, E. Hertz, and M. L. Schattenburg, "Scanning laser reflection tool for alignment and period measurement of critical-angle transmission gratings," Proc. - 32nd ASPE Annu. Meet. **10399**, 40–304 (2016).
34. Y. Shimizu, K. Uehara, H. Matsukuma, and W. Gao, "Evaluation of the grating period based on laser diffraction by using a mode-locked femtosecond laser beam," J. Adv. Mech. Des. Syst. Manuf. **12**(5), JAMDSM0097 (2018).
35. T. Photia, W. Temnuch, S. Srisuphaphon, N. Tanasanchai, W. Anukool, K. Wongrach, P. Manit, S. Chiangga, and S. Deachapunya, "High-precision grating period measurement," Appl. Opt. **58**(2), 270 (2019).
36. G. Dai, L. Koenders, F. Pohlenz, T. Dziomba, and H. U. Danzebrink, "Accurate and traceable calibration of one-dimensional gratings," Meas. Sci. Technol. **16**(6), 1241–1249 (2005).
37. D. A. Chernoff and D. L. Burkhead, "Roadmap for traceable calibration of a 5-nm pitch length standard," Metrol. Insp. Process Control Microlithogr. XXIV **7638**, 763837 (2010).

Optics EXPRESS

38. I. Ortlepp, J. Stauffenberg, and E. Manske, "Processing and analysis of long-range scans with an atomic force microscope (Afm) in combination with nanopositioning and nanomeasuring technology for defect detection and quality control," Sensors **21**(17), 5862 (2021).
39. Y. Shimizu, "Laser Interference Lithography for Fabrication of Planar Scale Gratings for Optical Metrology," Nanomanufacturing Metrol. **4**(1), 3–27 (2021).
40. F. Bienert, T. Graf, and M. Abdou Ahmed, "General mathematical model for the period chirp in interference lithography," Opt. Express **31**(4), 5334–5346 (2023).
41. Y. Jourlin, A. V. Tishchenko, C. Pedri, A. G. Zanzal, and J. Unruh, "Picometer-resolution assessment of the period constancy in a FBG phase mask," Opt. Fabr. Testing, Metrol. **5252**, 166 (2004).
42. Q. Liu, J. Wu, and W. Yang, "Fabrication of the linearly chirped phase mask for working in 248 nm wavelength," *2008 Int. Conf. Opt. Instruments Technol. Microelectron. Optoelectron. Devices Integr.* 7158, 71580F (2008).
43. Y.-J. Hung, C.-W. Kao, T.-C. Kao, C.-W. Huang, J.-J. Lin, and C.-C. Yin, "Optical spectrometer based on continuously-chirped guided mode resonance filter," Opt. Express **26**(21), 27515 (2018).